J Mater Sci (2011) 46:3151–3156
DOI 10.1007/s10853-010-5196-7

TaC precipitation behaviors in reduced activation martensitic steels

Z. X. Xia · C. Zhang · H. Lan · Z. G. Yang

Received: 20 August 2010 / Accepted: 13 December 2010 / Published online: 11 January 2011

Abstract The precipitation behaviors of TaC in reduced activation steels are investigated by the means of experimental and theoretical model. A continuous model based on the Langer–Schwartz theory for nucleation, growth, and coarsening was developed for both homogeneous and heterogeneous precipitation. Applying this model, an extensive data set (the precipitation size and density) including experimental and reported results has been well described. The effects of the thermodynamics parameters on the microstructure were discussed. TaC showed a low coarsening rate during tempering as the solubility of tantalum in the ferrite matrix is quite small with a value of 10^{-5} at 1023 K.

Introduction

For the Test Blanket Modules (TBMs) of the International Thermonuclear Experimental Reactor (ITER), reduced activation ferritic/martensitic (RAFM) steel is selected as the preferred candidate for the structural material [1, 2]. According to Klueh [1], reduced activation status could be achieved if the typical alloying elements Ni, Mo, Nb, Cu, and N were eliminated or restricted. Ta is used to substitute Nb in RAFM steels due to its superior irradiation properties. Meanwhile, Ta is more beneficial for toughness and high creep properties of the steel [3].

However, Ta is not generally used for commercial steels, and its precipitation behavior is unclear [4]. It is generally accepted that Ta exists in the nanoscale TaC precipitates in RAFM steels, the time exponent of coarsening of TaC precipitates is reported to be extremely small in RAFM steel [5–7], and the TaC precipitates are of great benefit to the creep properties [8]. Understanding the mechanism of TaC precipitation would contribute to predict its coarsening behaviors in a long period, which is more important for the service safety. The precipitation of NbC on dislocations [9] and grain boundaries [10] in ferrite has been simulated by the classical theory and Monte Carlo study, respectively. However, the experimental and modeling work of the TaC precipitation are hardly reported. This article will simulate the processing of the TaC precipitation in tempered RAFM steels.

Experimental

The designed steels were cast in a vacuum induction furnace. The ingots were heated at 1423 K and hot-rolled into square bars with 12 by 12 mm, and then homogenized for 48 h at 1473 K followed by natural cooling. The chemical composition of the steels is given in Table 1. Each grade is derived from reduced activation steel (9Cr2WVTa). In order to simplify the precipitation behavior, V and W are excluded from the original chemical composition of reduced activation steel. Heat treatment includes austenitizing at 1323 K for 1 h, followed by water quenching (WQ), then tempering at 1023 K for 3, 9, and 24 h, respectively, followed by air cooling (AC).

The transverse plane of tempered specimens was mechanically polished, and then electrochemically etched in methanol containing 10% Acetylacetone and 1% tetramethylammonium chloride. The procedure resulted in almost complete retention of carbides which were examined

Z. X. Xia · C. Zhang (✉) · H. Lan · Z. G. Yang
Key Laboratory of Advanced Materials of Ministry of Education, Department of Materials Science and Engineering, Tsinghua University, Beijing 100084, China
e-mail: chizhang@mail.tsinghua.edu.cn

Table 1 Chemical composition (mass fracture %) of tested steel

Heat	Fe	C	Mn	Cr	Ta	N	S	P	O
M1	BaL	0.12	<0.01	<0.01	0.14	0.0025	0.0064	<0.005	<0.002
M2	BaL	0.10	0.49	8.78	0.16	0.0290	0.0058	<0.005	<0.002

by FEI Sirion 200 SEM with EDAX. The carbides were extracted electrolytically using a water solution of 5% potassium chloride, 1% citric acid at the current density of 0.03 A/cm^2 and examined using X-ray diffraction (XRD using Cu Kα radiation). The tempered martensitic microstructure was investigated by a transmission electron microscopy (TEM, FEI-F20) accompanied with EDX. All specimens for metallography were examined on a plane vertical to the long length of the forged bars. The average size of TaC particles was calculated out of 10 TEM images for every result of tempering at 1023 K for 3, 9, and 24 h.

Experimental results

The SEM results have shown that two classes of TaC in M1 steel were identified as shown in Fig. 1. Numerous approximately spherical precipitates have also been found in M2 steel, as shown in Fig. 2. The change of size distribution and morphology of TaC phase with increasing tempering time seemed not to be obvious by SEM. In M1 steel, only TaC was observed by TEM with an increasing average diameter from 19 to 24 to 30 nm with increasing holding time during tempering, as shown in Fig. 3. For M2 steel, different precipitates, namely, M_7C_3, $M_{23}C_6$, and MX (Ta and V rich), were detected, similar to that found in a previous study [11]; furthermore, the average diameter of chromium carbides has also been reported to increase from 150 to 500 nm with increasing holding time [11], and the coarsening rate of chromium carbides seems to be higher than TaC phase in reduced activation steels. So there are three types of carbide TaC, Cr_7C_3, and $Cr_{23}C_6$ in M2 steel, as shown in Fig. 4. According to SEM/EDS analyses, the size of chromium carbides is one order of magnitude larger than that of TaC. The average diameter of TaC in M2 steel increased from 20 to 25 to 30 nm with increasing holding time (Fig. 5). The time exponent for TaC precipitated in RAFM steels is in agreement with the time exponent for TaC in the relation $D = 12t^{0.1}$ [5–7], the value of which is small, where the diameter D and the tempering time t are

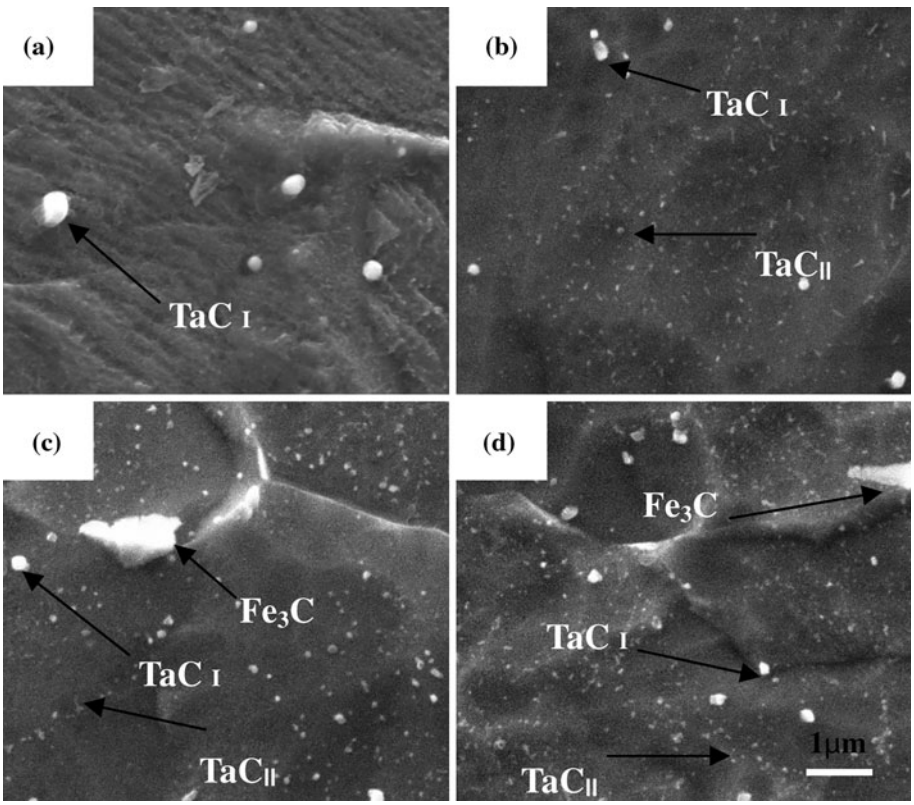

Fig. 1 Microstructure and precipitation behaviors of the M1 specimens tempered at 1023 K for **a** 0 h; **b** 3 h; **c** 9 h; **d** 24 h. TaCI: larger carbides with a diameter around 150 nm: this first population is undissolved carbides during austenitizing. TaCII: small carbides with a diameter around 20 nm: this second population includes precipitated tantalum carbides during tempering

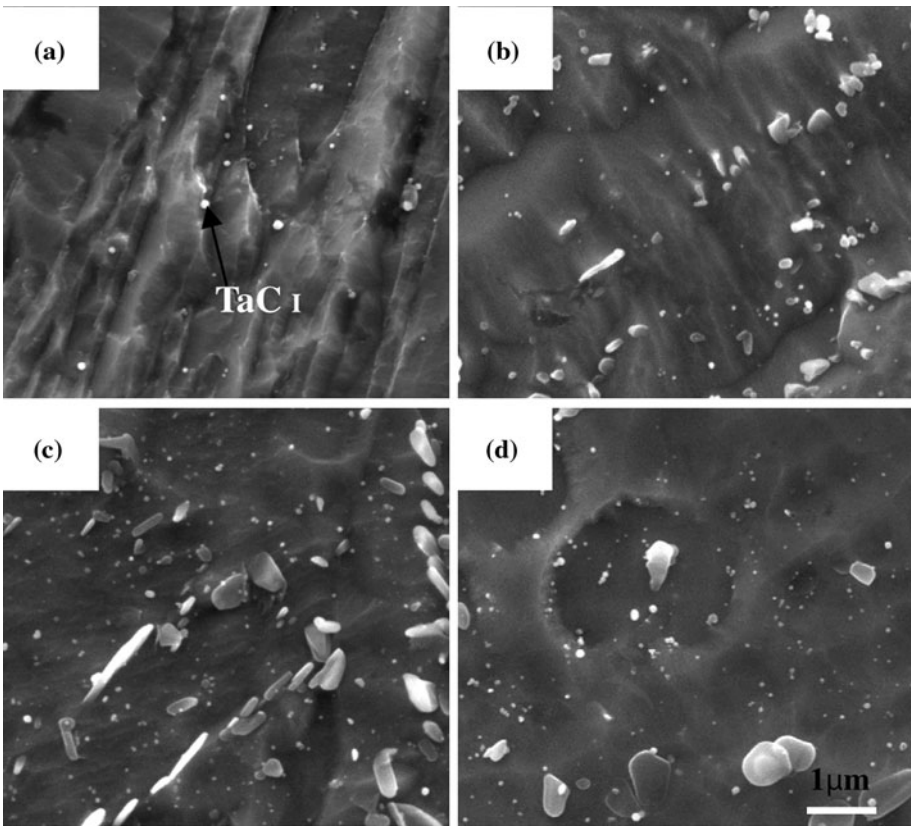

Fig. 2 Microstructure and precipitation behaviors of the M2 specimens tempered at 1023 K for **a** 0 h; **b** 3 h; **c** 9 h; **d** 24 h

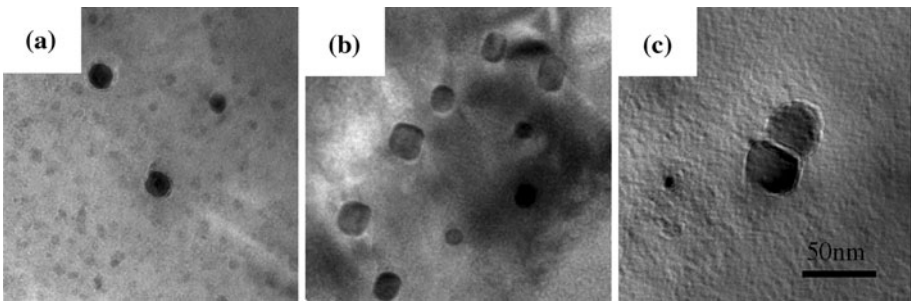

Fig. 3 TEM micrographs of TaC precipitates in M1 steel tempered at 1023 K for **a** 3 h, **b** 9 h, **c** 24 h

in nm and hour, respectively. Nucleation and growth of TaC are considered to occur simultaneously during isothermal aging in RAFM steels. One can also observe the new small TaC precipitation as it is coherent with martensitic matrix (bcc) after tempering for 9 h. TaC precipitates grow with $(200)_{TaC}$ and $(111)_{TaC}$ facets, see Fig. 6.

Discussion

Simulation method

The Langer–Schwartz model [12] was adopted to simulate the precipitation of TaC in tempered martensitic steels. The simulation process is under the following assumptions: (1) The composition of TaC is stoichiometric, whose thermodynamics is given by a simple solubility product. The diffusion coefficient of tantalum is very small compared to that of carbon. The precipitation reaction is purely controlled by the diffusion of tantalum, which means that the interface concentrations are given by a local equilibrium. (2) For the sake of simplicity, precipitates are assumed to be spherical. (3) During the early stage of nucleation and growth, small TaC precipitates are coherent with the Fe matrix. (4) Nucleation and growth are considered to occur simultaneously during isothermal aging in this system, which means that new precipitates can nucleate while existing precipitates are in their growing stage. In this nucleation and growth mode, the precipitate can be countered only when its radius is larger than the critical radius.

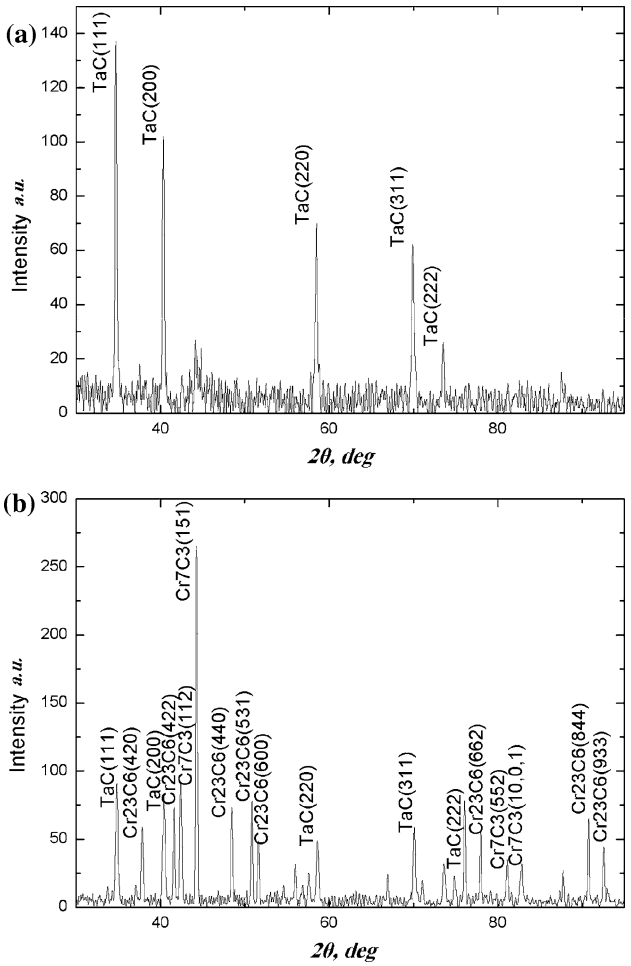

Fig. 4 X-ray diffraction patterns of extracted carbides from specimens tempered at 1023 K for 24 h **a** M1 steel, **b** M2 steel

The precipitate number N and the nucleation rate J are expressed as follows:

$$N = \int_{R^*}^{\infty} f(R)\mathrm{d}R \tag{1}$$

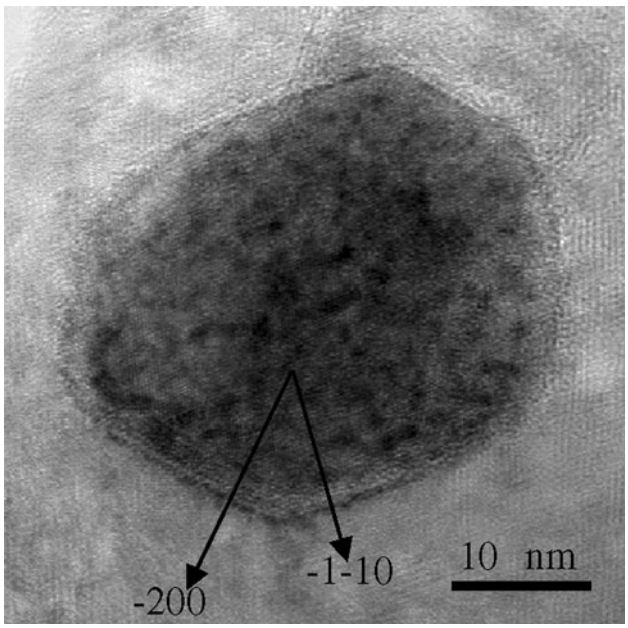

Fig. 6 HTEM micrographs of TaC in M1 steel tempered at 1023 K for 9 h

$$J = \int_{R^*}^{\infty} j(R)\mathrm{d}R \tag{2}$$

The time evolution of $f(R)$ which satisfies the continuity equation as follows:

$$\frac{\partial f(R)}{\partial t} = -\frac{\partial}{\partial R}(v(R)\cdot f(R)) + j(R) \tag{3}$$

$$\frac{\mathrm{d}N}{\mathrm{d}t} = J - f(R^*)\frac{\mathrm{d}R^*}{\mathrm{d}t} \tag{4}$$

where N is particle number, R^* is critical radius, $f(R)$ is size distribution, only precipitates with $R > R^*$ are to be counted as part of the precipitate phase (departure from LSW theory [12]). $v(R)$ and $j(R)$ denote the radial velocity

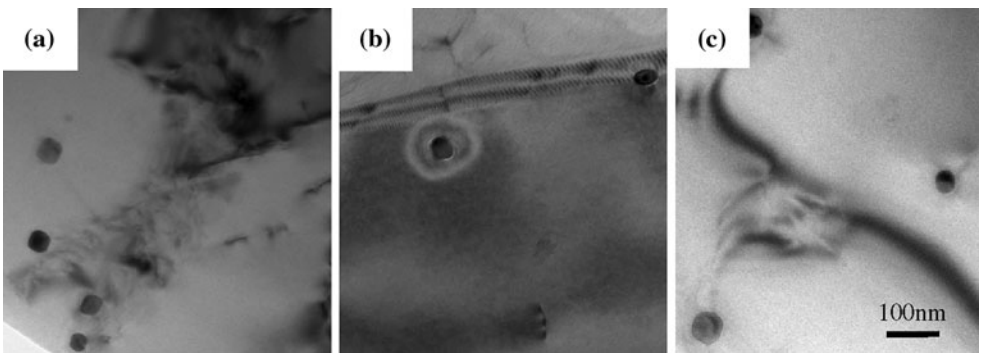

Fig. 5 TEM micrographs of TaC precipitates in M2 steel tempered at 1023 K for **a** 3 h, **b** 9 h, **c** 24 h

and distributed nucleation rate, respectively. Gibbs–Thomson equation

$$c_R = c_e \cdot \exp\left(\frac{2\sigma V_m}{R_g T} \cdot \frac{1}{R}\right)$$

$$R^* = \frac{2 \cdot \sigma \cdot V_m}{R_g T} \frac{1}{\ln \frac{\bar{c}}{c_e}} \quad (5)$$

The growth rate of precipitates is calculated by means of invariant field approximation.

$$\frac{dR}{dt} = v(R) = \frac{\bar{c} - c_R}{c_p - c_R} \frac{D}{R} \quad (6)$$

where c_e is tantalum equilibrium concentration in ferrite ahead of the interface, c_R is the concentration in the matrix at the boundary of the precipitate of radius R, σ is interface energy, R_g is molar gas constant, T is the absolute temperature, V_m is molar volume, D is diffusion coefficient of Ta, c_0 is bulk composition, $\bar{c}$ is mean concentration of the matrix, c_p is tantalum equilibrium concentration in TaC particles ahead of the interface.

According to the Eqs. 4 and 6, the modeling of the nucleation, growth, and coarsening could be described.

Model calibration and comparison with experimental results during isothermal aging

Empirical solubility product for carbon and tantalum solubility is presented in steels [13, 14]. The solubility is also accurately available according to Fe–Ta phase diagram [15]. The diffusion coefficient of Ta is based on Ref. [16]. A slight adjustment of value from this literature could be allowed. The dislocation density of quenched martensitic steel has been determined as 10^{15} m^{-2} [17]. σ for precipitation at dislocations is assumed to be the approximately same as σ of homogeneous precipitation, and the interfacial energy at 1023 K can be assumed to be 0.35 J/m^2 according to the previous study [18]. The activation energy for pipe diffusion along dislocations was estimated to be $0.7Q$ for α-Fe (Q is the activation energy of volume diffusivity) [19]. These data concerning TaC precipitation in RAFM steels tempered at 1023 K are given in Table 2.

The Ta mole fraction, precipitate mean radius and precipitate density from the experimental data and model predictions are shown in Fig. 7. The experimental results are well described by the model of precipitation on dislocations. The solubility of tantalum is 10^{-5} at 1023 K, which is perfectly coincided with the equilibrium volume fraction of tantalum calculated by this model, as shown in Fig. 7a. Figure 7b suggested the experimental and the reported precipitates size of TaC [7, 20, 21] is within the zone between homogeneous and heterogeneous precipitation. The precipitates size of TaC measured using XRD and TEM by Tamura et al. [7] is in good agreement with the model of homogenous precipitation, and even in better agreement with the model of precipitation on dislocations by Jayaram and Klueh [20], Kai and Klueh [21], and this experiment, though their difference is extremely small. Apart from the heterogeneous precipitation on dislocations, the relatively smaller TaC precipitates by homogenous precipitation may be neglected in TEM observations, but they could be detected by XRD, which probably resulted in the larger precipitates size of TaC measured by using TEM than that of XRD. As shown in Fig. 7b, the calculated precipitation density of TaC begins to increase rapidly when the incubation time is over. The incubation time is known to be proportional to the nucleus-matrix interfacial energy σ; thus, the uncertainty of σ has a relatively little influence on the incubation time of precipitation. However, the influence of σ, on the peak number is larger: a 10 pct increase of σ caused a decrease in the peak number of more than an order of magnitude provided that classical theory was used [17]. On the other hand, the diffusivity of Ta also has a large influence on the incubation time of precipitation, which becomes one order of magnitude less if the diffusivity is one order of magnitude greater. The nucleation at dislocations and in the matrix only is both in an early short period. The nucleation site number is less and the diffusivity is faster at dislocations; therefore, the precipitates density is less and the critical size can be achieved at a shorter holding time than that within the matrix, as shown in Fig. 7c. It also shows a good agreement with the previous data [20, 21]. The precipitation of TaC along the prior grain boundaries and packet boundaries is easier and faster than that within the matrix. Iseda et al. [22] assumed that the lattice misfit is large and the driving force needed to precipitate on boundaries is smaller. It is considered that MX carbonitrides do not grow fast during high-temperature creep due to the small solubility of Nb and V in the ferrite matrix [23]. Hence, it can be concluded that TaC precipitates also grow slowly during tempering as tantalum has a larger lattice misfit and a smaller solubility than that of Nb and V in the ferrite matrix according to the Narita's data [14].

Table 2 Data concerning TaC precipitation in RAFM steels tempered at 1023 K

b	V_m (m^3/mol)	a (m)	σ (J/m^2)	N_0	Q (J/mol)
0.317014	10.851×10^{-6}	0.3296×10^{-9}	0.35	1.0466×10^{25}	−252000

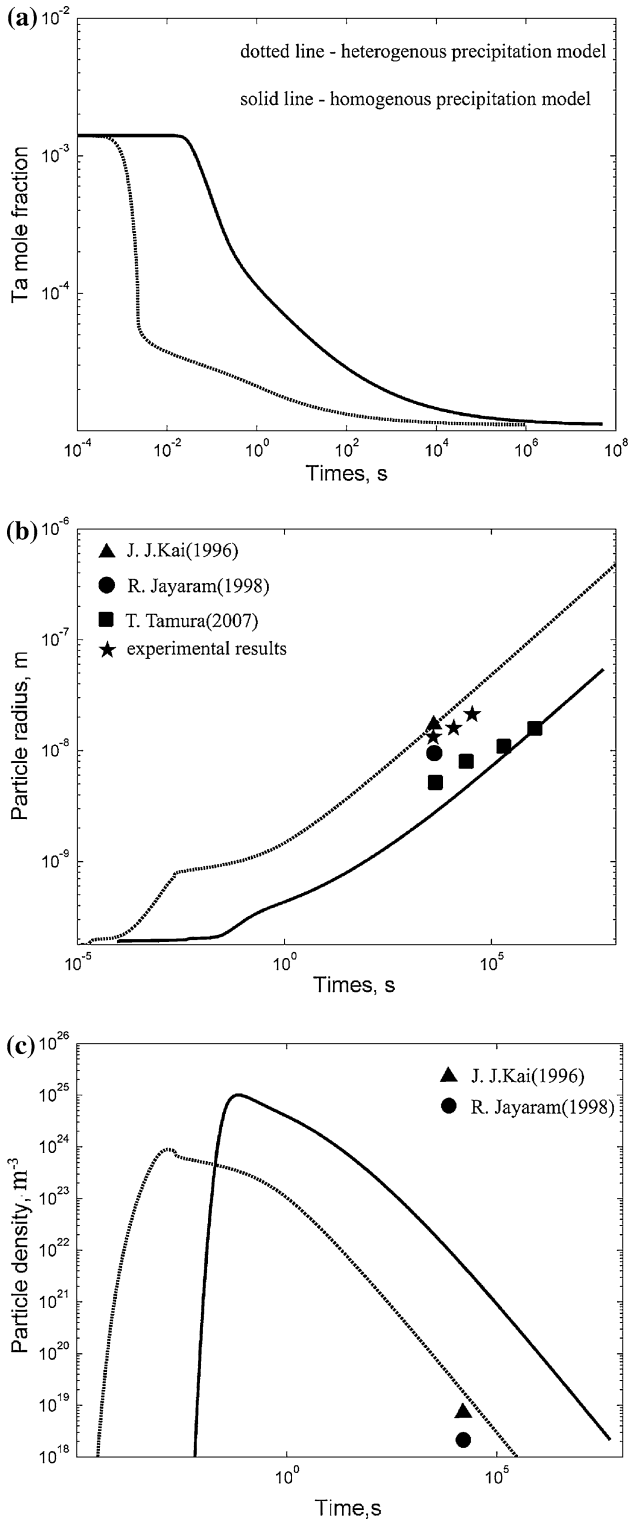

Fig. 7 Comparison between experimental and homogeneous and heterogeneous nucleation modeling results for the isothermal heat treatments. **a** Equilibrium volume fraction of tantalum, **b** particle radius, **c** particle density

Summary

A continuous model based on the Langer–Schwartz has been developed for both homogeneous and heterogeneous precipitation. The extensive experimental data set (the precipitation size and density) has been well described. The model can predict the effects of the thermodynamics parameters on the final microstructure. The results demonstrate that tantalum equilibrium concentration in ferrite ahead of the interface c_e especially has a strong influence on the precipitation size and density. c_e is quite small below 1023 K. This is one of the important reasons for the small time exponent of coarsening of TaC precipitates in reduced activation ferritic/martensitic steels.

Acknowledgements This study was carried out with great financial supports from National Basic Research Program of China (No. 2010CB731600) and National Natural Science Foundation of China (No. 51071090).

References

1. Klueh RL (2008) J Nucl Mater 378:159
2. Kimura A, Kasada R et al (2007) J Nucl Mater 367:60
3. Jinnan Yu, Huang Q, Wan F (2007) J Nucl Mater 367:97
4. Tanigawa H et al (2006) In: 21st fusion energy conference, International atomic energy agency, Oct. 16th–21st, Chengdu, China
5. Tamura M, Shinozuka K et al (2000) J Nucl Mater 283:667
6. Fernandez P, Lancha AM et al (2002) J Nucl Mater 307:495
7. Tamura M, Kusuyama H, Shinozuka K, Esaka H (2007) J Nucl Mater 367:137
8. Tanigawa H, Sakasegawa H, Hashimoto N, Klueh RL, Ando M, Sokolov MA (2007) J Nucl Mater 367:42
9. Perrard F, Deschamps A, Maugis P (2007) Acta Mater 55:1255
10. Hin C, Brechet Y, Maugis P, Soisson F (2008) Acta Mater 56:5653
11. Xia ZX, Zhang C et al (2010) Mater Sci Eng A 528:657
12. Langer JS, Schwartz AJ (1980) Phys Rev A 21:948
13. Tamura M, Shinozuka K, Masamura K, Ishizawa K, Sugimoto S (1998) J Nucl Mater 258:1158
14. Narita K, Koyama S (1966) Tetsu-to-Hagane 52:788
15. Smithells CJ (1992) Smithells metals reference book, 7th edn. Butterworth-Heinemann, Boston
16. Enomoto M (2000) Phase transformation in metals. Uchida Rokakuho, Tokyo, p 249
17. Zhang C, Enomoto M, Yamashita T, Sano N (2004) Metall Mater Trans A 35:1264
18. Yang ZG, Enomoto M (2002) Mater Sci Eng 332A:184
19. Peterson NL (1980) Grain boundary structure and kinetics. ASM, Metals Park, p 209
20. Jayaram R, Klueh RL (1998) Metall Mater Trans A 29:1551
21. Kai JJ, Klueh RL (1996) J Nucl Mater 230:116
22. Iseda A, Teranishi H, Masuyama F (1990) Tetsu-to-Hagane 76:1076
23. Ennis PJ, Zielinska-Lipec A, Wachter O, Czyrska-Filemonowicz A (1997) Acta Mater 45:4901